

Synthesis of g-C₃N₄/WO₃ Composites under Hydrothermal Conditions and Study of Their Photocatalytic Properties †

Ekaterina D. Medvedeva ¹, Daniil A. Kozlov ^{1,2} , Alexander O. Revenko ¹ and Alexey V. Garshev ^{1,3,*}

¹ Faculty of Materials Science, Lomonosov Moscow State University, Moscow 119991, Russia; medvedevaed@my.msu.ru (E.D.M.); kozlov@inorg.chem.msu.ru (D.A.K.); arevenko27@gmail.com (A.O.R.)

² Kurnakov Institute of General and Inorganic Chemistry, Russian Academy of Sciences, Moscow 119991, Russia

³ Faculty of Materials Science, Shenzhen MSU-BIT University, Shenzhen 518172, China

* Correspondence: garshev@inorg.chem.msu.ru

† Presented at the 4th International Online Conference on Nanomaterials, 5–19 May 2023;

Available online: <https://iocn2023.sciforum.net>.

Abstract: g-C₃N₄/WO₃ composites have drawn great interest in heterogeneous photocatalysis due to their effective separation of charge carriers at the contact with semiconductor phases. In this work, we have studied the effect of hydrothermal conditions on composites' structure and photocatalytic activities. Initial g-C₃N₄ was obtained using the classical melamine thermolysis approach. g-C₃N₄/WO₃ composites were synthesized under hydrothermal conditions from acidic tungstate solutions. Structure and composition changes in g-C₃N₄ were described using FTIR-spectroscopy and CHNO-analysis. The synthesized composites were characterized by powder XRD and STEM analysis, which showed WO₃ formation on the g-C₃N₄ surface. The photocatalytic activity was evaluated in the reaction of hydrogen peroxide generation from oxygen under UV irradiation. The obtained composites demonstrated up to three times higher photocatalytic activity than the individual semiconductor photocatalysts.

Keywords: photocatalysis peroxide generation; composite materials; graphitic carbon nitride; tungsten oxide; hydrothermal synthesis



Citation: Medvedeva, E.D.; Kozlov, D.A.; Revenko, A.O.; Garshev, A.V. Synthesis of g-C₃N₄/WO₃ Composites under Hydrothermal Conditions and Study of Their Photocatalytic Properties. *Mater. Proc.* **2023**, *14*, 17. <https://doi.org/10.3390/IOC2023-14536>

Academic Editor: Jian-Gan Wang

Published: 5 May 2023



Copyright: © 2023 by the authors. Licensee MDPI, Basel, Switzerland. This article is an open access article distributed under the terms and conditions of the Creative Commons Attribution (CC BY) license (<https://creativecommons.org/licenses/by/4.0/>).

1. Introduction

Photocatalysis has been attracting much attention due to its application in different global problems such as air [1] and water purification [2], generation of green fuels via water splitting [3], and CO₂ reduction [4]. One of the most popular photocatalysts actively studied recently is graphitic carbon nitride (g-C₃N₄), which demonstrates significant photocatalytic activity under visible light illumination and, moreover, is chemically and thermally stable [5]. Nevertheless, the efficiency of g-C₃N₄ is limited by the high possibility of photogenerated electron–hole pairs' recombination. One approach to improve g-C₃N₄ photocatalytic activity is the formation of composites with metal [6] or other semiconductor nanoparticles [7]. Commonly, tungsten oxide WO₃ is considered the best candidate for the creation of composites with g-C₃N₄ due to its band structure as well as its chemical and physical properties [8]. Furthermore, WO₃ is a great choice for the second complementary semiconductor to g-C₃N₄ for the construction of an efficient Z-scheme system. Thus, being contacted, WO₃ and g-C₃N₄ contribute to the separation of photogenerated charge carriers into different phases realizing the Z-scheme mechanism—holes drift to the WO₃ valence band and electrons to the g-C₃N₄ conduction band. This leads to spatial separation of oxidation and reduction processes, which increases photocatalytic activity.

To synthesize the g-C₃N₄/WO₃ composites methods of simultaneous heating [9] and hydrothermal treatment [10] are commonly used. The first one includes mixing precursors of each semiconductor and then annealing at their decomposition temperature. With

such annealing, catalytic decomposition of $g\text{-C}_3\text{N}_4$ by WO_3 is possible [11]. On the other hand, hydrothermal treatment of already obtained $g\text{-C}_3\text{N}_4$ in acidic tungstate solutions can be conducted. In that case, hydrolysis of carbon nitride might occur, which leads to the destruction of the initial structure. However, by varying the processing conditions, precipitation can be achieved without destroying the structure [10]. Overall, despite some challenges, both of these methods make it possible to achieve contact between semiconductor particles using a minimum number of synthesis steps.

The aim of the current research was to develop optimal conditions for the hydrothermal synthesis of $g\text{-C}_3\text{N}_4/\text{WO}_3$ composites. For successful synthesis, WO_3 nanoparticles should precipitate on the surface of $g\text{-C}_3\text{N}_4$ particles, and the structure of initial $g\text{-C}_3\text{N}_4$ should be intact. Moreover, the effect of hydrothermal conditions on the $g\text{-C}_3\text{N}_4$ structure was systematically studied. The obtained composites containing both phases had shown great photocatalytic activity, which was demonstrated to be more than three times exceeding the individual photocatalysts' activities.

2. Materials and Methods

2.1. Synthesis of $g\text{-C}_3\text{N}_4$

Initial $g\text{-C}_3\text{N}_4$ was synthesized using the classical thermolysis approach, where melamine (analytical grade, Sigma-Aldrich, Saint Louis, MO, USA) was chosen as a precursor. The melamine was placed in a closed corundum crucible and annealed under $550\text{ }^\circ\text{C}$ for four hours in the air. Synthesized products were cooled down at room temperature and had a characteristic yellow color.

To establish the optimal conditions of the composite's hydrothermal synthesis, experiments with $g\text{-C}_3\text{N}_4$ were carried out. Aqueous sol of $g\text{-C}_3\text{N}_4$ was obtained by 20 min ultrasonic treatment of 300 mg $g\text{-C}_3\text{N}_4$ in 40 mL of deionized water. Then, the pH level was adjusted to 2–5 using HCl solution (35% solution, Rushim, Moscow, Russia), and the obtained sol was placed in a Teflon-lined stainless autoclave. The autoclave was placed in a muffle oven at a temperature of $180\text{ }^\circ\text{C}$ for 2–12 h. At the end of the treatment, the obtained samples were centrifuged at 10,000 rpm for 10 min, and then the precipitate was washed several times with distilled water and dried at a temperature of $60\text{ }^\circ\text{C}$.

2.2. Synthesis of $g\text{-C}_3\text{N}_4/\text{WO}_3$

The synthesis of the composites was carried out under hydrothermal conditions. For this purpose, 40 mL of a stable sol containing 300 mg of $g\text{-C}_3\text{N}_4$ powder was treated ultrasonically for 20 min. Then, a certain amount of sodium tungstate (analytical grade, Sigma-Aldrich) and sodium sulfate (analytical grade, Sigma-Aldrich) was added to achieve the desired WO_3 content in the final composites (12.5, 37.5, 62.5, and 87.5 wt. %). After ultrasonic treatment, the suspension was adjusted to $\text{pH} = 1.5$ using 1M H_2SO_4 (analytical grade, Rushim) and placed in a Teflon-lined stainless autoclave with a volume of 60 mL. Hydrothermal treatment was carried out at a temperature of $180\text{ }^\circ\text{C}$ for 4 h. Then, the resulting mixture was centrifuged at 10,000 rpm for 10 min, and the precipitate was washed several times with distilled water, and dried at a temperature of $60\text{ }^\circ\text{C}$. The obtained samples were marked as $g\text{-C}_3\text{N}_4/\text{WO}_3$ (x%), where x corresponds to theoretical weight WO_3 content.

The amount of $g\text{-C}_3\text{N}_4$ in the synthesized composites was determined using thermogravimetric analysis. The sample was placed in a corundum crucible and annealed under $450\text{ }^\circ\text{C}$ for 2 h in the air. At the end of the annealing, all $g\text{-C}_3\text{N}_4$ burned down, and in the crucible there was only WO_3 . Based on the ratio of the masses of the sample before and after annealing, the mass fraction of $g\text{-C}_3\text{N}_4$ was calculated.

2.3. Material Characterization

X-ray powder diffraction (PXRD) study was performed on a D/MAX 2500 (Rigaku, Tokyo, Japan) diffractometer with a rotating anode in reflection mode (Bragg–Brentano geometry) using $\text{CuK}\alpha_{1,2}$ radiation and a graphite monochromator. FTIR spectra were

recorded on an ALPHA (Bruker, Bremen, Germany) Fourier-transform IR spectrometer in the range of 400–4000 cm^{-1} in attenuated total reflectance mode. CHNO elemental analysis was performed on a 2400 Series II (PerkinElmer, Houston, TX, USA) CHNS/O elemental analyzer. Scanning transmission electron microscopy (STEM) images were collected using an Amber GMH (Tescan, Brno, Czech Republic) microscope operated at an accelerating voltage of 30 kV using bright field (BF) and high-angle dark field (HADF) detectors.

To study the kinetics of photocatalytic hydrogen peroxide formation, 0.2 mL of ethanol and 0.3 mL of 0.1 M phosphate buffer solution were added to 2.5 mL of an aqueous suspension of photocatalyst with a concentration of 0.1 mg/mL. The suspension was exposed to irradiation of a UV lamp (wavelength 366 nm) of the TLC Visualizer 2 (CAMAG, Muttenz, Switzerland) instrument with stirring. The concentration of the evolved hydrogen peroxide was determined by the specific enzymatic reaction of 3,3',5,5'-tetramethylbenzidine (TMB) oxidation by horseradish peroxidase. For this purpose, 60 μL aliquots were taken each 5 min and added to a 96-well plate with a mixture of 204 μL of 0.1 M phosphate buffer, 6 μL of 5×10^{-5} M solution of horseradish peroxidase, and 30 μL of 10^{-2} M alcoholic TMB solution. The concentration of oxidized TMB was determined by spectrophotometry using a SPECTROstar Nanospectrometer (BMG LabTech GmbH, Ortenberg, Germany) with an accuracy of ± 0.003 optical units.

3. Results and Discussion

3.1. Characterization of $g\text{-C}_3\text{N}_4$

Changes in the structure of $g\text{-C}_3\text{N}_4$ samples treated under hydrothermal conditions were analyzed using FTIR spectroscopy. The FTIR spectra of the $g\text{-C}_3\text{N}_4$ sample obtained by melamine thermolysis and the sample obtained after 12 h of hydrothermal treatment are shown in Figure 1. The spectra prove the formation of the initial $g\text{-C}_3\text{N}_4$ structure and consist of typical $g\text{-C}_3\text{N}_4$ vibrations, such as C=N bonds (1625 cm^{-1}), vibrations of aromatic rings ($1550\text{--}1300 \text{ cm}^{-1}$), and residues of non-condensed intermediate products containing -NH and -NH₂ groups ($3300\text{--}3050 \text{ cm}^{-1}$). In comparison with FTIR spectra of the initial $g\text{-C}_3\text{N}_4$, a significant change in structure has been determined after hydrothermal treatment (Figure 1B), which could be caused by a formation of a new phase. Most likely, the new phase is melamine cyanurate, since there are characteristic vibrations of it on the FTIR spectra: vibrations of -NH₂ (3396 cm^{-1}), formations of hydrogen-bonding vibrations between -NH₂/-NH groups (3234 cm^{-1}), and vibrations of carbonyl group C=O (1782 cm^{-1}). The results of CHNO analysis are also shown in Figure 1. It shows an increase in oxygen and hydrogen content in the sample after hydrothermal treatment when compared to that of the initial material. It also confirms a change in $g\text{-C}_3\text{N}_4$ structure during hydrolysis. Thus, the maximum time of hydrothermal treatment preventing graphitic carbon nitride hydrolysis was defined as the minimum time for WO₃ formation.

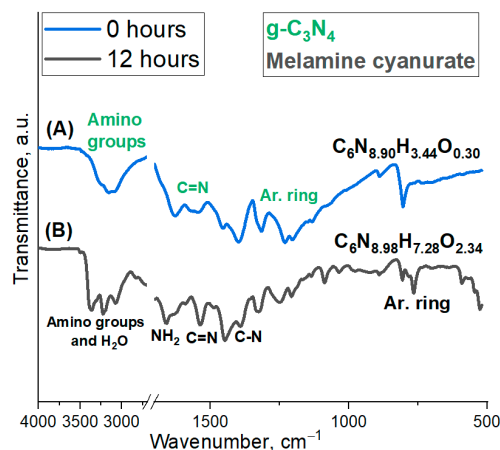


Figure 1. FTIR spectra of (A) $g\text{-C}_3\text{N}_4$ obtained by melamine thermolysis and (B) $g\text{-C}_3\text{N}_4$ obtained after 12 h of hydrothermal treatment.

3.2. Characterization of $g\text{-C}_3\text{N}_4/\text{WO}_3$

Based on PXRD results (Figure 2), $g\text{-C}_3\text{N}_4/\text{WO}_3$ composites contain both tungsten oxide and graphitic carbon nitride phases. Two diffraction peaks at 13.3° and 27.5° corresponding to (100) and (002) planes confirm the presence of the $g\text{-C}_3\text{N}_4$ phase in the samples. There are no peaks on the pattern that could be attributed to the phase of melamine cyanurate or other derivative phases of carbon nitride, which means that the $g\text{-C}_3\text{N}_4$ structure was not significantly changed during the hydrothermal treatment.

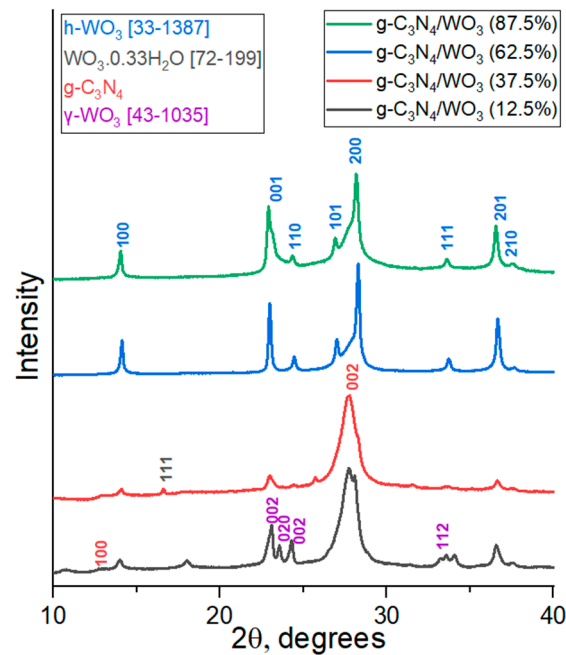


Figure 2. XRD patterns of $g\text{-C}_3\text{N}_4/\text{WO}_3$ samples after hydrothermal treatment.

Phase analysis of $g\text{-C}_3\text{N}_4/\text{WO}_3$ composites indicates the presence of several phases of tungsten oxide depending on the tungstate concentration in the synthesis. The composites with the maximum content of tungsten oxide contain WO_3 with a hexagonal crystalline structure (ICDD No. 33-1387). An increase of $g\text{-C}_3\text{N}_4$ amount leads to hydrated tungsten oxide $\text{WO}_3 \cdot 0.33\text{H}_2\text{O}$ crystallization (ICDD No. 72-199), and at the maximum concentration of $g\text{-C}_3\text{N}_4$ (in the sample with $\omega(\text{WO}_3) = 12.5\%$) the main tungsten-containing phase is monoclinic $\gamma\text{-WO}_3$ (ICDD No. 43-1035). Thereby, the addition of $g\text{-C}_3\text{N}_4$ during hydrothermal treatment of a sodium tungstate in acidic medium affects the phase composition of the deposited tungsten oxide.

To evaluate a tungsten oxide distribution over the $g\text{-C}_3\text{N}_4$ particles' surface, STEM images were taken (Figure 3). On HADF STEM images it is clear that large tungsten oxide particles are uniformly distributed and cover plate-like $g\text{-C}_3\text{N}_4$ particles. Thus, the observed contact between WO_3 and $g\text{-C}_3\text{N}_4$ nanoparticles can benefit efficient photogenerated charge carriers transfer, which results in an increase in the photocatalytic activity of the obtained composites.

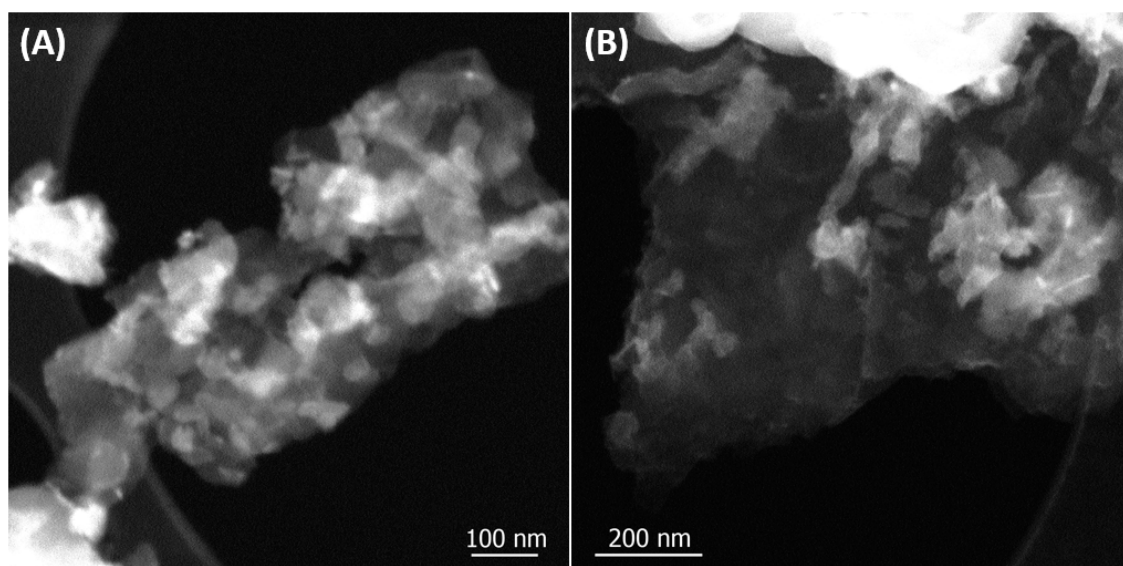


Figure 3. HADF STEM images of $g\text{-C}_3\text{N}_4/\text{WO}_3$ sample containing (A) $\omega(\text{WO}_3) = 37.5\%$ and (B) $\omega(\text{WO}_3) = 12.5\%$ after hydrothermal treatment.

Photocatalytic activity of the obtained $g\text{-C}_3\text{N}_4/\text{WO}_3$ samples was studied in the reaction of the photocatalytic reduction of oxygen dissolved in a water–alcohol mixture into hydrogen peroxide. The results of these experiments are shown in Table 1. With an increase in tungsten oxide mass fraction in $g\text{-C}_3\text{N}_4/\text{WO}_3$ composites up to 12.5%, there was a significant increase in the rate of hydrogen peroxide formation (up to 6.8×10^{-4} M/min). It is more than three times higher than the rate of hydrogen peroxide formation by the individual semiconductor photocatalysts $g\text{-C}_3\text{N}_4$ and WO_3 obtained under similar conditions. This increase in photocatalytic activity can be explained by the formation of the contact between semiconductor particles. That confirms the composite formation, in which the photocatalytic reaction proceeded according to the Z-scheme with spatial separation of charge carriers. At the same time, an increase in the tungsten oxide fraction in composites to more than 50% leads to a significant decrease in photocatalytic activity, caused by total loading of the composite’s surface with WO_3 particles.

Table 1. The photocatalytic activity of $g\text{-C}_3\text{N}_4/\text{WO}_3$ composites obtained by hydrothermal treatment.

Sample Name	$g\text{-C}_3\text{N}_4$ Content, wt. %	Tungsten Oxide Content, wt. %	H_2O_2 Formation Rate, M/min
$g\text{-C}_3\text{N}_4/\text{WO}_3$ (0%)	100	0	2.0×10^{-4}
$g\text{-C}_3\text{N}_4/\text{WO}_3$ (12.5%)	92	8 ($\gamma\text{-WO}_3$)	6.8×10^{-4}
$g\text{-C}_3\text{N}_4/\text{WO}_3$ (25%)	80	20 ($\gamma\text{-WO}_3$ and $\text{WO}_3 \cdot 0.33\text{H}_2\text{O}$)	5.7×10^{-4}
$g\text{-C}_3\text{N}_4/\text{WO}_3$ (50%)	47	53 (h- WO_3)	1.9×10^{-4}
$g\text{-C}_3\text{N}_4/\text{WO}_3$ (100%)	0	100 (h- WO_3)	2.0×10^{-4}

4. Conclusions

The present study has provided valuable insights into the formation and photocatalytic properties of $g\text{-C}_3\text{N}_4/\text{WO}_3$ composites synthesized under hydrothermal conditions. Our results indicate that hydrolysis of $g\text{-C}_3\text{N}_4$ occurs under hydrothermal conditions, which, according to FTIR spectroscopy and CHNO-analysis, leads to the formation of melamine cyanurate in the samples with a long treatment time. The method of $g\text{-C}_3\text{N}_4/\text{WO}_3$ composites formation, which includes hydrothermal treatment of deposited hydrated tungsten oxide on $g\text{-C}_3\text{N}_4$, was found to be effective. Under hydrothermal conditions, hexagonal

WO₃ crystallizes in composites with a high content of tungsten oxide, whereas an increase in the g-C₃N₄ fraction leads to the formation of WO₃·0.33H₂O and monoclinic modification of WO₃. Synthesized composites demonstrate significant photocatalytic activity in the reaction of hydrogen peroxide formation, exceeding the activity of individual WO₃ and g-C₃N₄ nanoparticles obtained under similar conditions by more than three times. Our findings suggest that the developed method of composite synthesis holds great promise for applications in various heterogeneous photocatalytic processes.

Author Contributions: Investigation, data curation, E.D.M.; investigation, software, methodology, D.A.K.; investigation, A.O.R.; writing—original draft preparation, E.D.M. and D.A.K.; writing—review and editing, A.O.R. and A.V.G.; validation, conceptualization, supervision, A.V.G. All authors have read and agreed to the published version of the manuscript.

Funding: This research received no external funding.

Institutional Review Board Statement: Not applicable.

Informed Consent Statement: Not applicable.

Data Availability Statement: Not applicable.

Acknowledgments: The research was carried out using the equipment of the MSU Shared Research Equipment Centre “Technologies for obtaining new nanostructured materials and their complex study” and purchased by MSU in the frame of the Equipment Renovation Program (National Project “Science and Universities”). The measurements were performed using the equipment of the Joint Research Centre (JRC PMR) IGIC RAS and supported by IGIC RAS state assignment (Ministry of Higher Education and Science of the Russian Federation).

Conflicts of Interest: The authors declare no conflict of interest.

References

1. Katsumata, K.; Motoyoshi, R.; Matsushita, N.; Okada, K. Preparation of graphitic carbon nitride (g-C₃N₄)/WO₃ composites and enhanced visible-light-driven photodegradation of acetaldehyde gas. *J. Hazard. Mater.* **2013**, *260*, 475–482. [[CrossRef](#)] [[PubMed](#)]
2. Rokicka-Konieczna, P.; Markowska-Szczupak, A.; Kusiak-Nejman, E.; Morawski, A.W. Photocatalytic water disinfection under the artificial solar light by fructose-modified TiO₂. *Chem. Eng. J.* **2019**, *372*, 203–215. [[CrossRef](#)]
3. Ng, B.; Putri, L.K.; Kong, X.Y.; Teh, Y.W.; Pasbakhsh, P.; Chai, S. Z-Scheme photocatalytic systems for solar water splitting. *Adv. Sci.* **2020**, *7*, 1903171. [[CrossRef](#)] [[PubMed](#)]
4. Huang, S.; Long, Y.; Ruan, S.; Zeng, Y.J. Enhanced Photocatalytic CO₂ Reduction in Defect-Engineered Z-Scheme WO_{3-x}/g-C₃N₄ Heterostructures. *ACS Omega* **2019**, *4*, 15593–15599. [[CrossRef](#)] [[PubMed](#)]
5. Yao, J.; Zhang, M.; Yin, H.; Luo, Y.; Liu, X. Improved photocatalytic activity of WO₃/C₃N₄: By constructing an anchoring morphology with a Z-scheme band structure. *Solid State Sci.* **2019**, *95*, 105926. [[CrossRef](#)]
6. Gao, G.; Jiao, Y.; Waclawik, E.R.; Du, A. Single Atom (Pd/Pt) Supported on Graphitic Carbon Nitride as an Efficient Photocatalyst for Visible-Light Reduction of Carbon Dioxide. *J. Am. Chem. Soc.* **2016**, *138*, 6292–6297. [[CrossRef](#)] [[PubMed](#)]
7. Reli, M.; Huo, P.; Šihor, M.; Ambrožová, N.; Troppová, I.; Mat, L.; Lang, J.; Svoboda, L.; Ku, P.; Ritz, M.; et al. Novel TiO₂/C₃N₄ Photocatalysts for Photocatalytic Reduction of CO₂ and for Photocatalytic Decomposition of N₂O. *J. Phys. Chem. A* **2016**, *120*, 8564–8573. [[CrossRef](#)] [[PubMed](#)]
8. Fu, J.; Xu, Q.; Low, J.; Jiang, C.; Yu, J. Ultrathin 2D/2D WO₃/g-C₃N₄ step-scheme H₂-production photocatalyst. *Appl. Catal. B Environ.* **2019**, *243*, 556–565. [[CrossRef](#)]
9. Cui, L.; Ding, X.; Wang, Y.; Shi, H.; Huang, L.; Kang, S. Facile Preparation of Z-scheme WO₃/g-C₃N₄ Composite Photocatalyst with Enhanced Photocatalytic Performance under Visible Light. *Appl. Surf. Sci.* **2016**, *391*, 202–210. [[CrossRef](#)]
10. Yang, M.; Hu, S.; Li, F.; Fan, Z.; Wang, F.; Liu, D.; Gui, J. The influence of preparation method on the photocatalytic performance of g-C₃N₄/WO₃ composite photocatalyst. *Ceram. Int.* **2014**, *40*, 11963–11969. [[CrossRef](#)]
11. Zhang, X.; Wang, X.; Meng, J.; Liu, Y.; Ren, M.; Guo, Y.; Yang, Y. Robust Z-scheme g-C₃N₄/WO₃ heterojunction photocatalysts with morphology control of WO₃ for efficient degradation of phenolic pollutants. *Sep. Purif. Technol.* **2021**, *255*, 117693. [[CrossRef](#)]

Disclaimer/Publisher’s Note: The statements, opinions and data contained in all publications are solely those of the individual author(s) and contributor(s) and not of MDPI and/or the editor(s). MDPI and/or the editor(s) disclaim responsibility for any injury to people or property resulting from any ideas, methods, instructions or products referred to in the content.